N88-11613

FIRST RESULTS ON QUIET AND MAGNETIC GRANULATION FROM SOUP

A. Title, T. Tarbell (Lockheed PARL), and the SOUP Team

(L. Acton[1], D. Duncan[1], S. Ferguson[1], M. Finch[1], Z. Frank[1], G. Kelly[1], R. Lindgren[1], M. Morrill[1], T. Pope[1], R. Reeves[1], R. Rehse[1], R. Shine[1], K. Topka[1], G. Simon[2], J. Harvey[3] J. Leibacher[3], W. Livingston[3], L. November[4], J. Zirker[4])

[1]*Lockheed Palo Alto Research Laboratory, Dept. 91-30, Bldg. 256, 3251 Hanover Street, Palo Alto, CA 94304, U.S.A.*
[2]*Air Force Geophysics Laboratory, Sunspot, NM 88349, U.S.A.*
[3]*National Solar Observatory, Tucson, AZ 85718 U.S.A.*
[4]*National Solar Observatory, Sunspot, NM 88349, U.S.A.*

ABSTRACT

The flight of SOUP on Spacelab 2 allowed the collection of time sequences of diffraction limited (0.5 arc second) granulation images with excellent pointing (0.003 arc seconds) and completely free of the distortion that plagues groundbased images. The p-mode oscillations are clearly seen in the data. Using fourier transforms in the temporal and spatial domain we have shown that the p-modes dominate the autocorrelation lifetime in magnetic regions. When these oscillations are removed the autocorrelation lifetime is found to be 500 seconds in quiet and 950 seconds in magnetic regions. In quiet areas exploding granules are seen to be common. It is hard to find a granule that does not explode or is not affected by an explosion. We speculate that a significant fraction of granule lifetimes are terminated by nearby explosions. Using local correlation tracking techniques we have been able to measure horizontal displacements, and thus transverse velocities, in the intensity field. In quiet sun it is possible to detect both super- and mesogranulation. Horizontal velocities are as great as 1000 m/s and the average velocity is 400 m/s. In magnetic regions horizontal velocities are much less, about 100 m/s.

I. Introduction

In the traditional model solar granulation is considered to be convective overshoot, in which the convective cells have a center to center distance of about 2 arc seconds and a lifetime of 4 to 16 minutes. In previous studies the lifetime has been highly dependent on whether the measurement technique averaged over ensembles of granules or isolated individual features. There have been some indications that granulation is slightly different in magnetic field regions and near sunspots, but there is still controversy on this point. On average the picture is that a granule is a bright central region of upflow, with a diameter of 1.5 arc seconds, surrounded by a darker region of downflow. The picture of granulation before the flight of SOUP has been excellently reviewed in "Solar Granulation" by Bray, Loughhead, and Durrant (1984).

The picture emerging from the analysis of the SOUP data is qualitatively different from the traditional model. However, at this point in time we cannot define granule evolution. The definition of granular evolution is complex because there exists in the solar surface a hierarchy of intensity fluctuations, from the p-mode oscillations with scales of many tens of arc seconds and large phase velocities to apparent surface waves with scales at or below the resolution limit and low or zero phase velocities. There are also local phenomena, which involve areas with radii of a few to ten arc seconds, such as the well-known exploding granules (Namba, 1986) which seem to be much more pervasive in the SOUP data than previously noted. It is difficult to find a point in the movies that does not "explode" or is clearly not affected by a nearby event. Other time evolving patterns exist that probably have a different physical origin than exploders. All of the wave fields and the local phenomena, of course, coexist in the intensity field we have called granulation. A single image does not begin to reveal the richness in the solar surface.

The granulation pattern is embedded in systematic flows with spatial scales from ten to at least forty arc seconds, and lifetimes long compared to a single thirty minute orbital observing period. Some of the flow fields probably are the meso and supergranulation, but other patterns may also exist.

In regions with significant magnetic field the surface flow patterns are considerably less vigorous, but not significantly less complex. The granulation pattern is statistically more stable, there is lower modulation in the intensity field, the wave patterns are diminished in amplitude as are the velocities of the steady flows, and exploding granules are much less common; but most of the phenomena seen in quiet sun can also be found in the magnetic regions.

The SOUP instrument on Spacelab 2 (SL 2) collected granulation data spanning a period of about 16 hours. The images are very uniform in quality and are distortion free. Using the ESA Instrument Pointing System (IPS) and an internal fast guider, image stability of 0.003 arc seconds RMS was achieved. An ideal data set was collected for movie analysis. We have created about 100 processed movies (15,000 processed frames) from three original digital image sequences. Image processing techniques have included spatial smoothing, running averages, median filtering, spatial and spatial-temporal fourier filtering, blink comparison, color overlays, and differencing. The processed images are recorded permanently on optical disks. The optical disks can be studied using a normal video monitor and a computer controlled video disk player.

We have spent many hours viewing the various movies. It is extremely unfortunate that there is not a convenient method for publishing them. Most of the topics reported here are based upon impressions gained from the movies. The eye-brain system is a subtle tool for acquiring information from movie presentations. However, developing quantitative procedures to describe some of these impressions is difficult and requires extensive calculations.

At the current stage of the data analysis, we are still sorting out what we have observed in movies, and analyzing the results of numerical processes we have applied. So far no

combination of algorithms has produced a convincing definition of a granule or the process of granule evolution. However, some of the investigations have been sufficiently quantitative to provide useful measures of the phenomena we observe in the solar surface. In the sections below we will report on the state of the analysis of granulation in quiet and magnetic sun as inferred from different analysis techniques.

II. Observations

The data used for this report were all collected on film using the Solar Optical Universal Polarimeter (SOUP) which operated on the flight of Spacelab 2 (Title *et al.* , 1986). The original images are 140 × 250 arc seconds and are taken in a thousand angstrom band centered at 6000ÅFor this preliminary report we have studied two digitized subsections, a 40 × 40 arc second quiet sun region, and a 60 × 60 arc second pore region. The pores are part of AR 4682 at approximately S15, W31 ($\mu = 0.83$). Because of limitations of the processing computer and our image display system, all digital images are 256 x 256 pixels. This corresponds to 0.161 and 0.234 arc second per pixel for the quiet and pore regions, respectively. The images are separated by 10 seconds in time and cover 1650 seconds. The results reported here are all from orbit 110 (19:10:35 to 19:38:07 GMT on 5 August 1985.)

III. Autocorrelation Measurements

One of the standard methods of determining lifetime of an intensity pattern is from the width of its autocorrelation (AC) function. Here we define the temporal autocorrelations of the intensity function as

$$AC(\tau) = \frac{\langle \delta I(x,y,t_0)\ \delta I(x,y,t_0+\tau) \rangle}{\langle \delta I^2(x,y,t_0) \rangle}$$

where x and y are the spatial coordinates, t_0 is the reference time, and τ the time separation. The brackets indicate an average over space, and

$$\delta I(x,y,t) = I(x,y,t) - \langle I(x,y,t) \rangle$$

where here the brackets indicate an average over space and time.

Previous AC lifetime measurements of granulation have ranged from 3 to 7 minutes with an average of about 6 minutes. Figure 1 shows the autocorrelation function measured in a number of recent studies (Mehltretter, 1978) compared with results from our data. As can be seen from the figure the agreement is good. The lifetime, as measured by the time for the correlation to drop to $1/e$ (.37) is about 5 minutes.

Our data for figure 1 were obtained from an area of about 350 square arc seconds (SAS). When smaller areas are examined the AC functions look quite different. Figure 2 (solid)

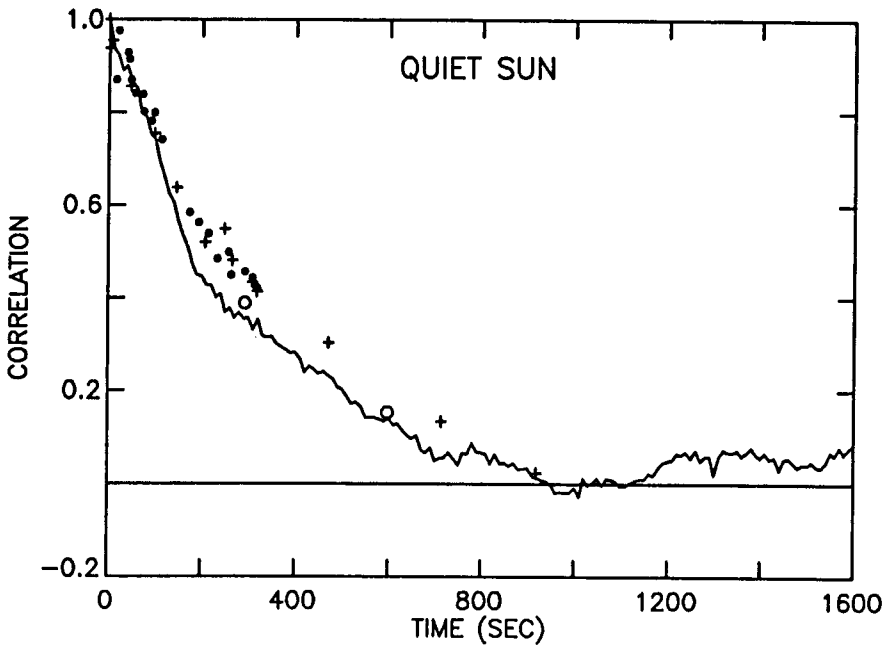

Fig. 1 Comparison of SOUP (solid) autocorrelation measurements with previously published results.

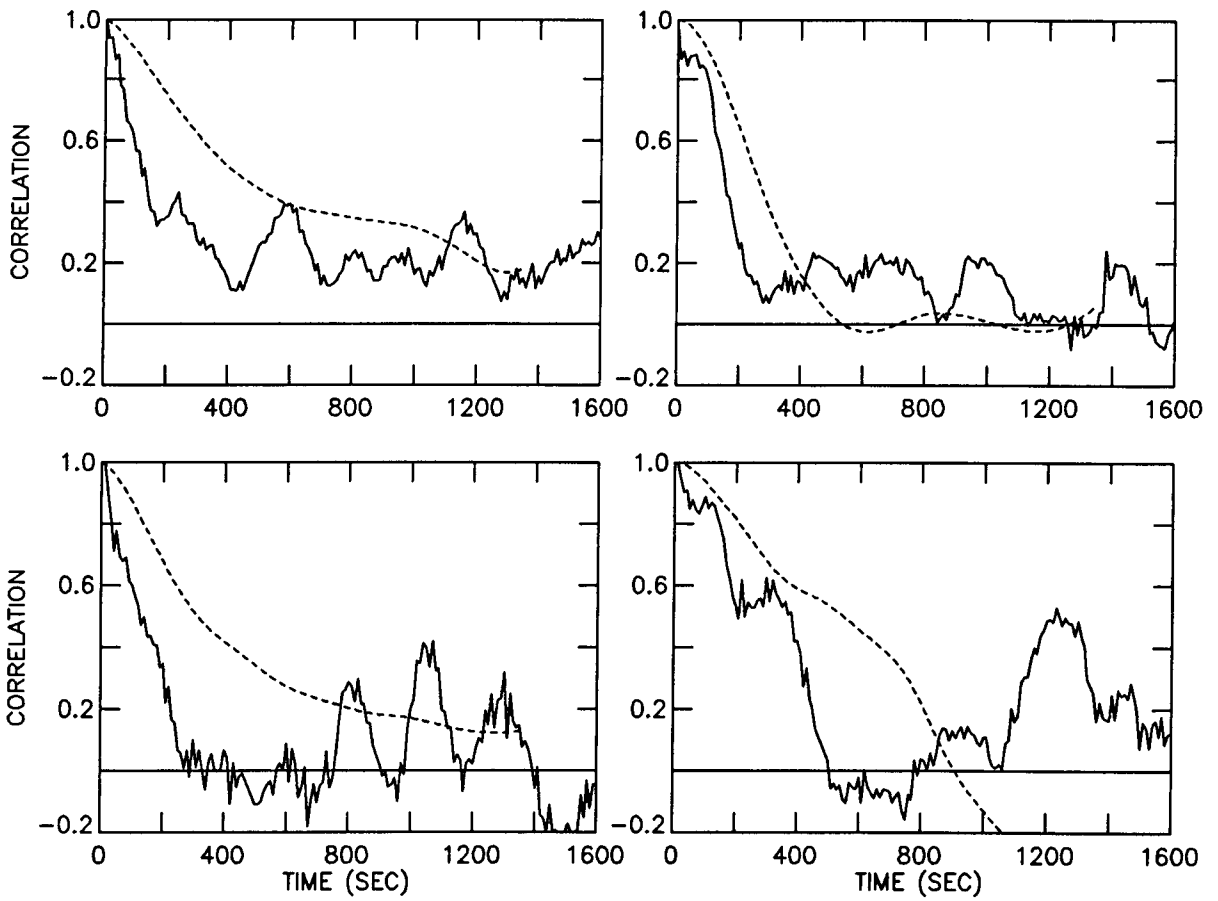

Fig. 2 AC(τ) in four 6×6 arc second regions (solid). These exhibit oscillations due to the solar p-modes. Dashed lines show AC(τ) for the same regions after subsonic filtering.

shows the AC functions generated from four 26 SAS areas. In these smaller regions the AC functions do not drop monotonically, but rather exhibit oscillations with periods of 3 to 6 minutes (depending on the region). This suggests that the five minute oscillation is affecting the correlation lifetime, which is not too surprising as it is strongly present in the granulation movies. The average AC over a sufficiently large region does not oscillate because a range of periods is present.

To remove the effect of the five minute oscillation we have applied what we call a subsonic fourier filter to the time sequence of quiet sun images. The original sequence of images is fourier transformed from a function of x, y, and t into a transformed function of k_x, k_y, and ω. The subsonic filter is defined by a cone

$$\omega = v \times k$$

in $k - \omega$ space, where k and ω are spatial and temporal angular frequencies and v is a velocity. All fourier components inside the cone (i.e., with phase velocities less than v) are retained, while all those outside are set to zero. A value of $v = 3$ km/s, well below the sound speed, 7 km/s, is used. For this value of v, the velocity cone is totally inside the fundamental and, of course, all of the overtones of the five minute oscillation. That is, it lies below the p-mode ridges in the well known $k - \omega$ diagram of the power spectrum of the solar velocity field. Therefore, it should include virtually all local phenomena, but exclude any waves with phase velocities greater than 3 km/sec.

Figure 3 shows a $k - \omega$ power spectrum for this data with the ridge pattern and the 3 km/s line overlayed. Clearly this filter excludes the power in the ridge pattern.

A subsonic filtered movie exhibits very little five minute oscillation. As seen from figure 2 (dashed) the AC functions created from subsonic filtered data for the individual regions have the oscillations strongly suppressed. Figure 4 shows the AC of 350 SAS for original (solid) and subsonic filtered (dashed) images. The AC lifetime of the subsonic data is greater by 50 percent than the original – a lifetime of 410 versus 270 seconds.

In order to observe the effect of magnetic field on the granulation pattern the SOUP images have been aligned with National Solar Observatory (Tucson) magnetograms taken just before and just after the SOUP data. Registration was accomplished by visual blink comparison of NSO continuum images and SOUP images. By registering the small pores and the spot present in both images, alignment to about 2 arc second accuracy was possible. The NSO continuum images and magnetograms are themselvesy registered to better than one arc second. Figure 5 shows the magnetogram contours (white) overlayed on the pore region. The boxes (black) in the figure are the regions selected for AC function analysis.

Twelve 36 SAS regions were selected to be inside the 70 gauss contour of the magnetograms, but well outside of pores. Shown in figure 6 are the AC functions for the original (solid) and the subsonic filtered (dashed) data for four of these regions. Figure 7 shows the sum

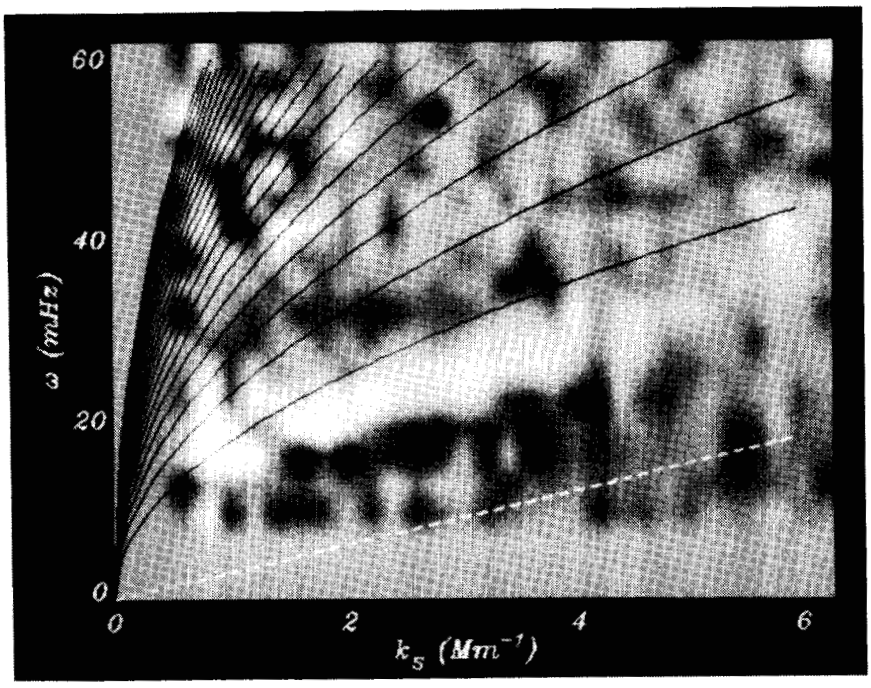

Fig. 3 $k - \omega$ diagram showing power in this data and the position of ridge pattern from other measurements (solid), and the line $\omega = 3k$ (dashed).

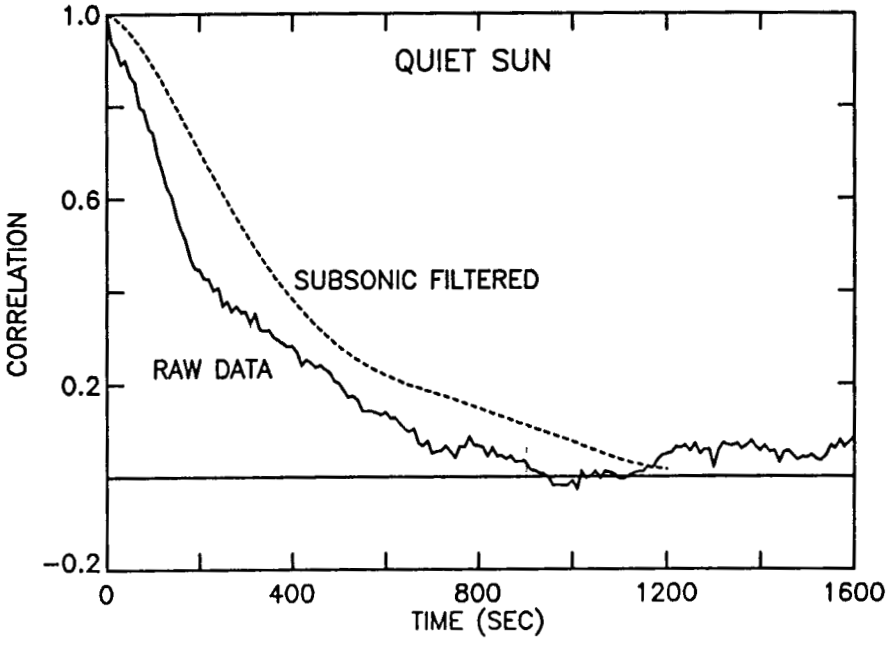

Fig. 4 AC functions for 350 SAS of quiet sun for original data (solid) and subsonic filtered data (dashed).

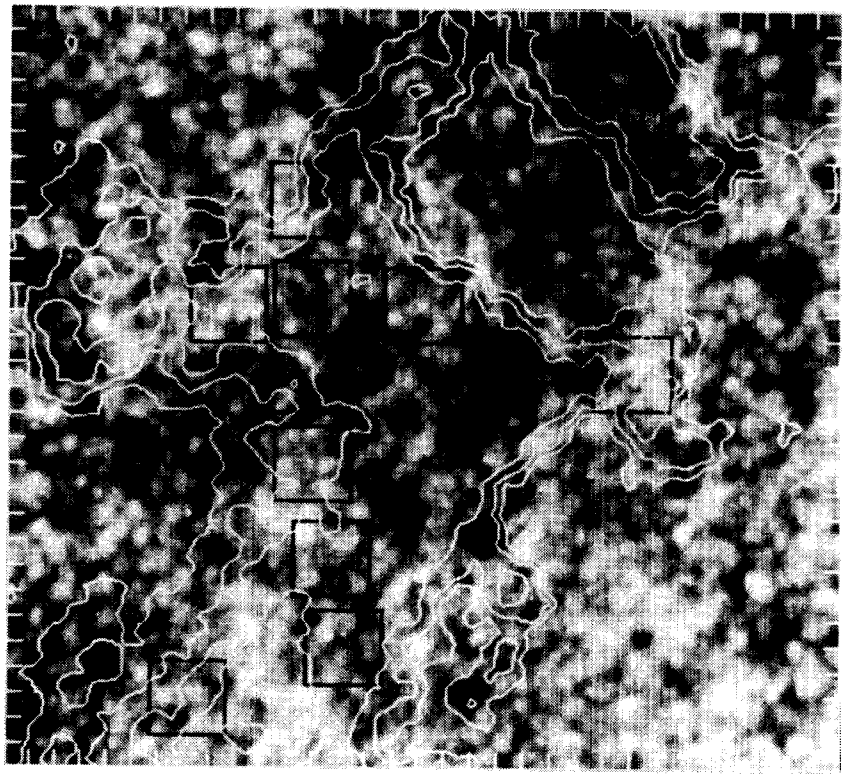

Fig. 5 Image of the pore region with magnetic contours overlayed. The contour levels are −75 and −270 gauss. The black boxes indicate regions used for constructing autocorrelation functions. Ticks are separated by one arc second.

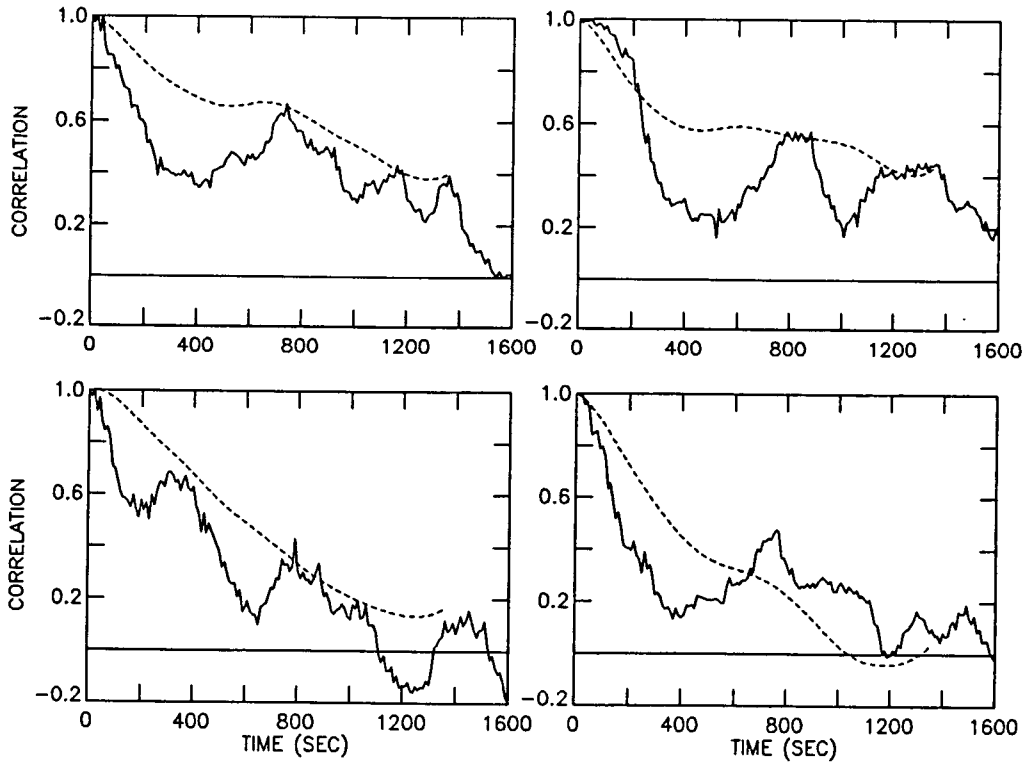

Fig. 6 AC functions for four magnetic regions using original (solid) and subsonic data (dashed).

ORIGINAL PAGE IS
OF POOR QUALITY

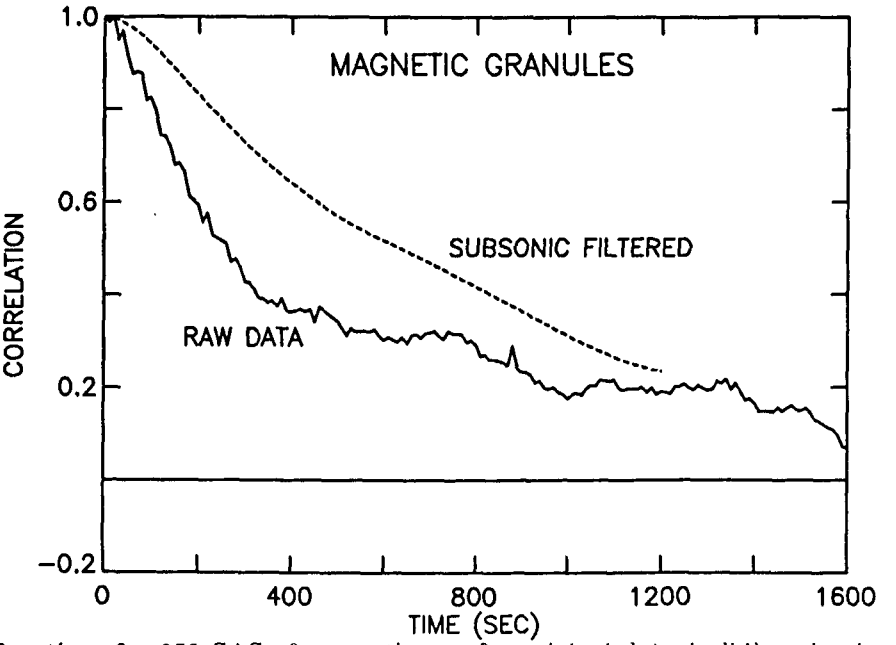

Fig. 7 AC functions for 350 SAS of magnetic sun for original data (solid) and subsonic filtered data (dashed).

of the AC's for the twelve regions for original (solid) and subsonic filtered (dashed) data. The lifetime from the subsonic data is a factor of two greater than the original data – 890 versus 420 seconds.

In magnetic regions the AC lifetime is dominated by the five minute oscillation and when this oscillation is removed the AC lifetime increases by about a factor of two. In quiet sun the effect of the subsonic filtering is much less. The removal of the effects of the five minute oscillation allows the autocorrelation technique to demonstrate that the convective pattern is significantly more stable in magnetic field regions than in quiet sun.

The temporal autocorrelation functions discussed above compare sets of spatially aligned images as a function of time and yield information related to feature lifetime. Spatial autocorrelation functions compare the same image with different spatial offsets and yield information on the spatial scale of the image. Here we define the spatial AC function as

$$AC(\Delta) = \frac{\langle \delta I(x,y,t)\ \delta I(x+\Delta,y,t)\rangle}{\langle \delta I^2(x,y,t)\rangle}$$

where Δ is the spatial offset. Figures 8a and 8b show (solid) the spatial AC's for quiet and magnetic sun, respectively. For a wide variety of patterns the half width at half maximum (HWHM) of the correlation function is related to the pattern size, r_0, by (Mosher,1977)

$$r_0 = 1.2 \times \text{HWHM}.$$

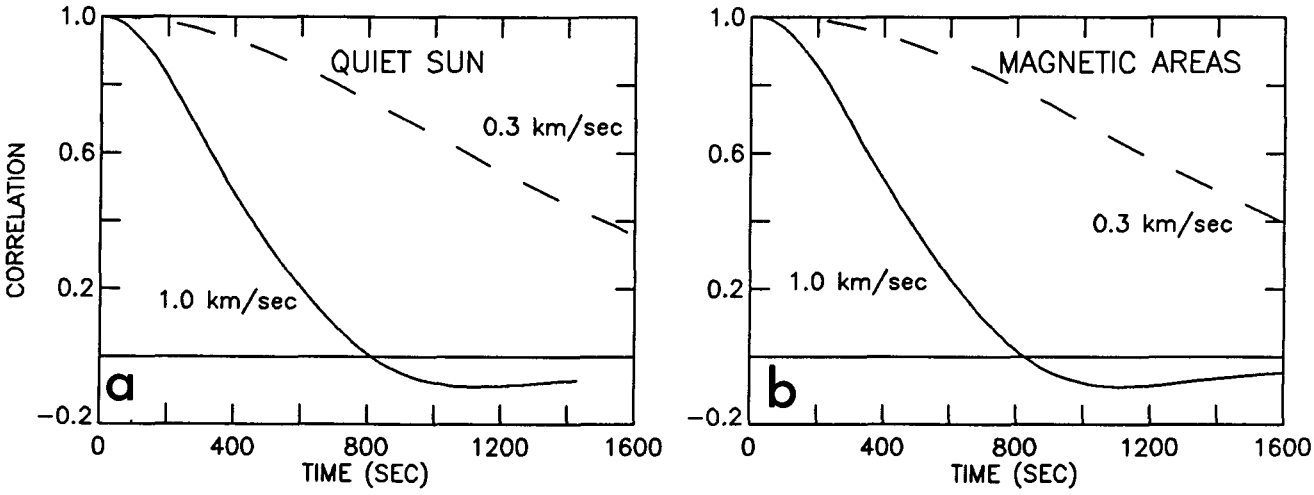

Fig. 8 Spatial autocorrelation functions for quiet (a) and magnetic sun (b). Solid curves curves are labeled 1 km/s to represent the fact that this curve would be generated by an infinite lifetime structure moving at 1 km/s. Dashed curves show the spatial AC functions for unchanging images displaced at 0.3 km/s.

The radius of the average structure in the quiet and magnetic regions is 450 and 500 km (diameters of 1.25 and 1.4 arc seconds), respectively. This suggests that on average the structures in the quiet and magnetic regions are about the same size.

The spatial AC functions can also be used to understand the effect of flows on the lifetime data because the displacement field can be interpreted as the result of a flow field. That is,

$$\Delta = v \times t.$$

The solid curves in figure 8 are labeled 1 km/s and can be interpreted as the temporal AC function of an intensity field of infinite lifetime that is moving at a constant velocity of 1 km/sec. Shown dashed in the same figure are curves corresponding to a displacement rate of 0.3 km/sec. The flow lifetime T_f, the time required for the flow to cause the spatial AC to drop to $1/e$, is just

$$T_f = \frac{AC_{1/e}}{v_f},$$

where v_f is the flow velocity. The value of $AC_{1/e}$ is 450 km for quiet sun and 500 km for magnetic.

The presence of a flow field will cause the measured lifetime from the temporal AC function to underestimate the lifetime of the granulation. Roughly the lifetimes as measured by the temporal AC functions, the actual lifetime, and the flow lifetime from the spatial AC functions are related by

$$1/T_m = \sqrt{(1/T_a)^2 + (1/T_f)^2},$$

or

$$T_a = \frac{T_m \times T_f}{\sqrt{T_f^2 - T_m^2}},$$

where T_a is the actual lifetime of the granules and T_m is the measured lifetime from the temporal AC function. This equation limits the flow lifetime to the measured lifetime, and therefore sets an upper limit on the average flow velocity. For quiet and magnetic sun the maximum flow velocities permitted by the observations are 1.1 and 0.5 km/s, respectively.

Using local correlation techniques (described below), we have measured the average flow velocities for quiet and magnetic sun to be 400 and 200 m/s, respectively. Correcting for the flow field yields "corrected" quiet and magnetic granule lifetimes of 440 and 950 seconds, respectively. Measurements of the velocity of individual granules has been done for the quiet sun (described below) and an average velocity of 0.9 km/s has been found. This corrects the AC lifetime to 710 seconds in quiet sun. The AC lifetime data is summarized in Table 1.

Table 1.

	Original	Subsonic	Steady Flow Correlation	Feature Flow Correlation
Quiet	270s	410s	440s	710s
Magnetic	420s	890s	950s	–

IV. Intensity Fluctuations

It is clear from the movies of the pore region that the oscillations and other intensity fluctuations are reduced in the magnetic field areas. (Reduced amplitude Doppler velocities in magnetic regions have long been observed.) Figures 9a and 9b show the mean intensity and the RMS intensity fluctuation as a function of position averaged over the entire movie. Brighter areas correspond to higher average intensities and higher RMS fluctuations respectively. Comparison of 9b, the RMS fluctuation map, and figure 5, the magnetic contour map overlaped on the pore image, shows that the RMS fluctuation tends to be lower in magnetic field regions. Figure 10 shows the mean RMS fluctuation versus

ORIGINAL PAGE IS
OF POOR QUALITY

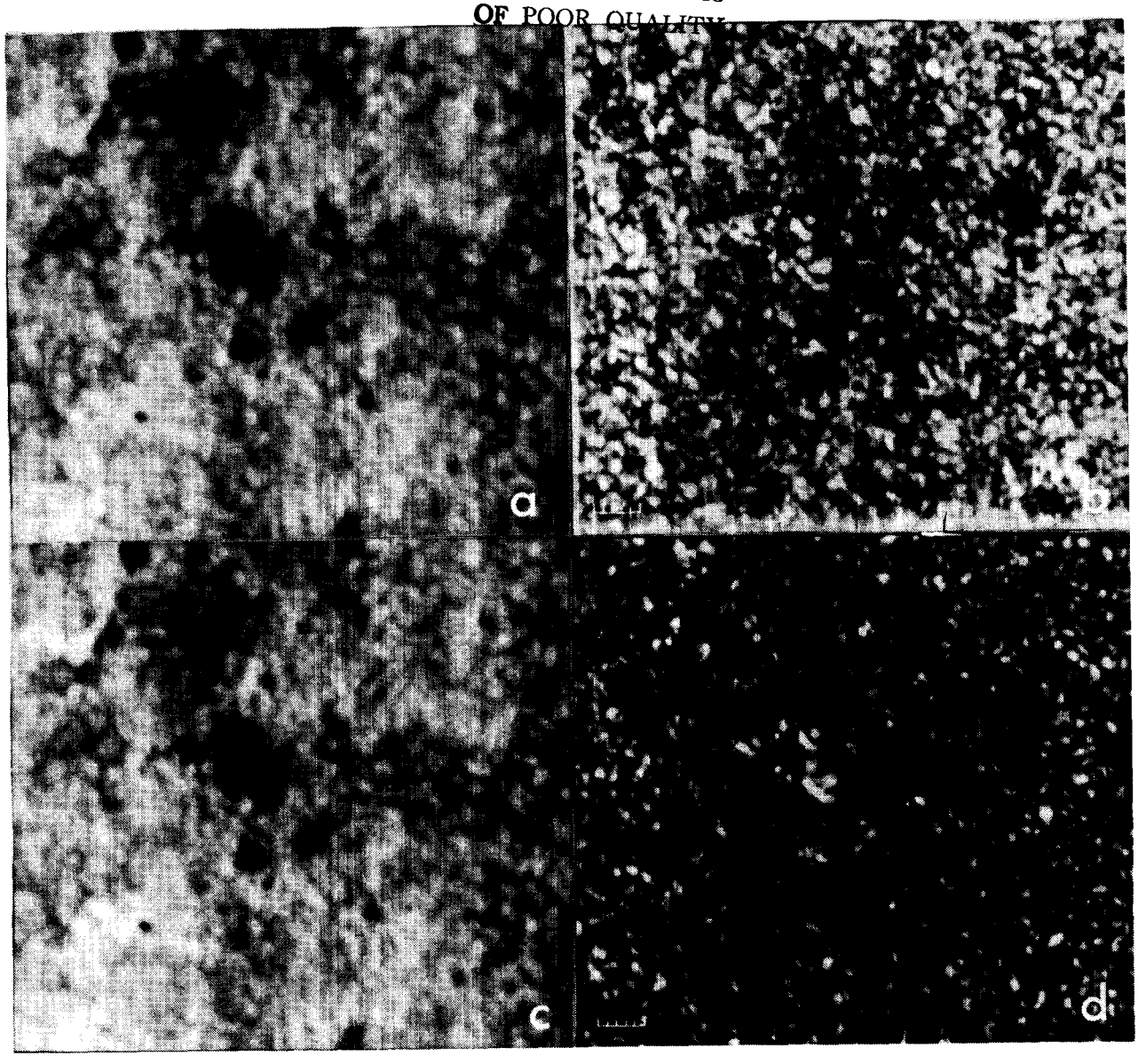

Fig. 9 A and B show the mean intensity and the RMS intensity fluctuation, respectively, for the original data in the pore region. C and D are similar images for the subsonic data for the pore region. The scale is marked in arc seconds.

magnetic field strength. Although the data is matched pixel by pixel, there is probably an offset error of several arc seconds and the resolution of the two images differ by a factor of at least four, so this good relationship suggests that the presence of a magnetic field affects a reasonable area of the granulation pattern.

Figures 9c and 9d show the mean and RMS fluctuations formed from the subsonic data set. Figures 9a and 9c are visually identical which shows that the removal of the periodic variations has almost no effect on the mean. Figures 9b and 9d, however, differ significantly.

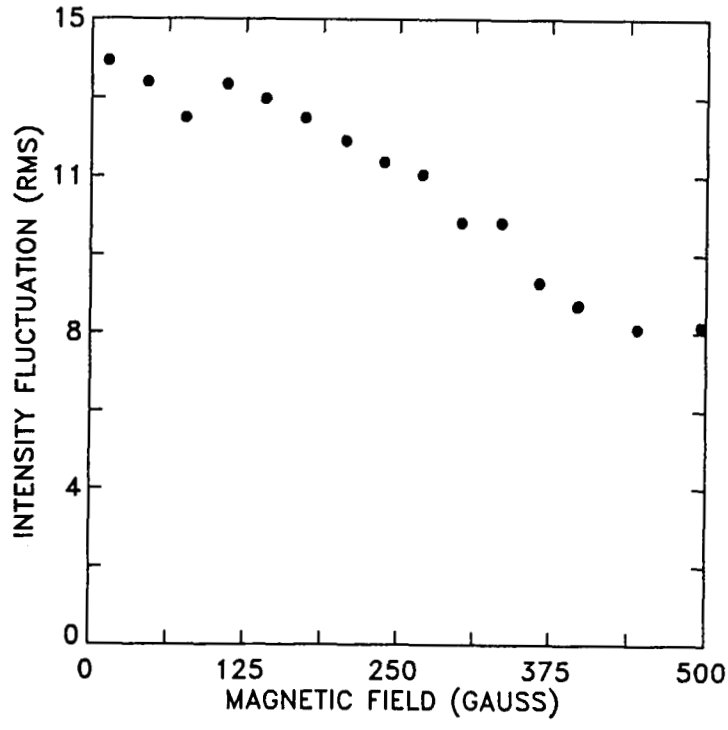

Fig. 10 Plot of the mean of the RMS intensity fluctuation at a particular value of the field versus magnetic field.

Most of the bright areas in RMS from the original data are considerably reduced in intensity in the subsonic RMS image. This refects the efficient removal of the five minute oscillation by the subsonic filter.

The higher average intensity and lower RMS fluctuation in magnetic regions are exactly what should be expected given the AC measurements described above and again strongly suggests that the magnetic field significantly changes the convective pattern.

V. Granule Tracking

Because granules move and change shape the autocorrelation method underestimates granule lifetimes. Another technique for determining lifetime is to track individual granules. The standard approach has been to find a granule on a master frame and then to track it as long as possible on following and preceding images. The weakness of such procedures is the biased selection of the tracked granules. Since our data are free of seeing we have tried to develop unbiased computer procedures for following granules.

The first step toward tracking granules is to identify them in all the images of a movie. We have tried two families of approaches. One is based on finding locally brightest points, and the other on finding borders which surround locally brighter areas. Or to put it another way, we have explored techniques to find granule centers directly by identification, and

indirectly by finding their boundaries and inferring a center in the middle of an enclosed area.

All center finding algorithms are based on exploring a local neighborhood and finding the brightest point in that area. Centers are located by subjecting every point in the image to the common test. Shown in figures 11a and 11b are a typical granulation frame and the same frame marked with the centers located by a center finding process. The average number of granules identified by center finders is 500 in a 1600 SAS area of quiet sun, or 31 granules per 100 SAS. This result for the granule density is about the mean of the value found by previous observers (Wittmann, 1979).

The lane finding procedure is much more sophisticated. It isolates local bright areas by surrounding them with a boundary lane. Granule centers are located at the center of gravity of the individual holes in the lane net. Figure 11c shows the quiet sun frame (figure 11a) overlaid by the lane net and its implied centers. About 1000 centers were found by the lane finding procedure, or 63 granules per 100 SAS.

A comparison of the center and lane finding results is shown in figure 11d, where the granulation mesh is shown shaded wherever a granule center was not found in the mesh cell. The shaded region in figure 11d covers 22 percent of the area of the image, but it contains as many cells as the other 78 percent of the image. (With very few exceptions mesh cells have no more than one "center found" granule in them.)

If we adjust the number of granules from the center finding process for the fact that they occupy only 78 percent of the area, then the granule density becomes 40 per 100 SAS. The granule density obtained from the center finding process and the area-corrected center finding process bracket the published values of the granule density. Mesh fragments in shaded areas have a density of 140 per 100 square arc seconds. With the assumption that granules are in a roughly hexagonal close packed pattern, the granule center-to-center distance is 1.9, 1.7, and 0.9 arc seconds for densities of 32, 40, and 140 granules per 100 SAS.

The agreement in the granule density gives us some confidence that the granule center finding procedure is a reasonable approach to finding granules. The factor of two higher densities found by the lane finder algorithm suggests that, in addition to finding granules, it also finds smaller granule "fragments".

Given a set of images with granule centers marked, it should be straightforward to identify the center of the same granule on sequential movie frames. We make this identification if two granule centers are within M arc seconds of each other on frames separated by 30 seconds in time. Proceeding this way through a time series of frames, we obtain a set of granule centers marked in three dimensional space-time. Each granule corresponds to a connected path in space-time, which we call a "string"; a string has a well-defined duration in time and an average slope (transverse velocity) may also be computed. Figure 12 contains plots of the number of granules with string duration t as a function of t, for M's of 0.5 and 1 arc second for center and lane found granules in original and subsonic

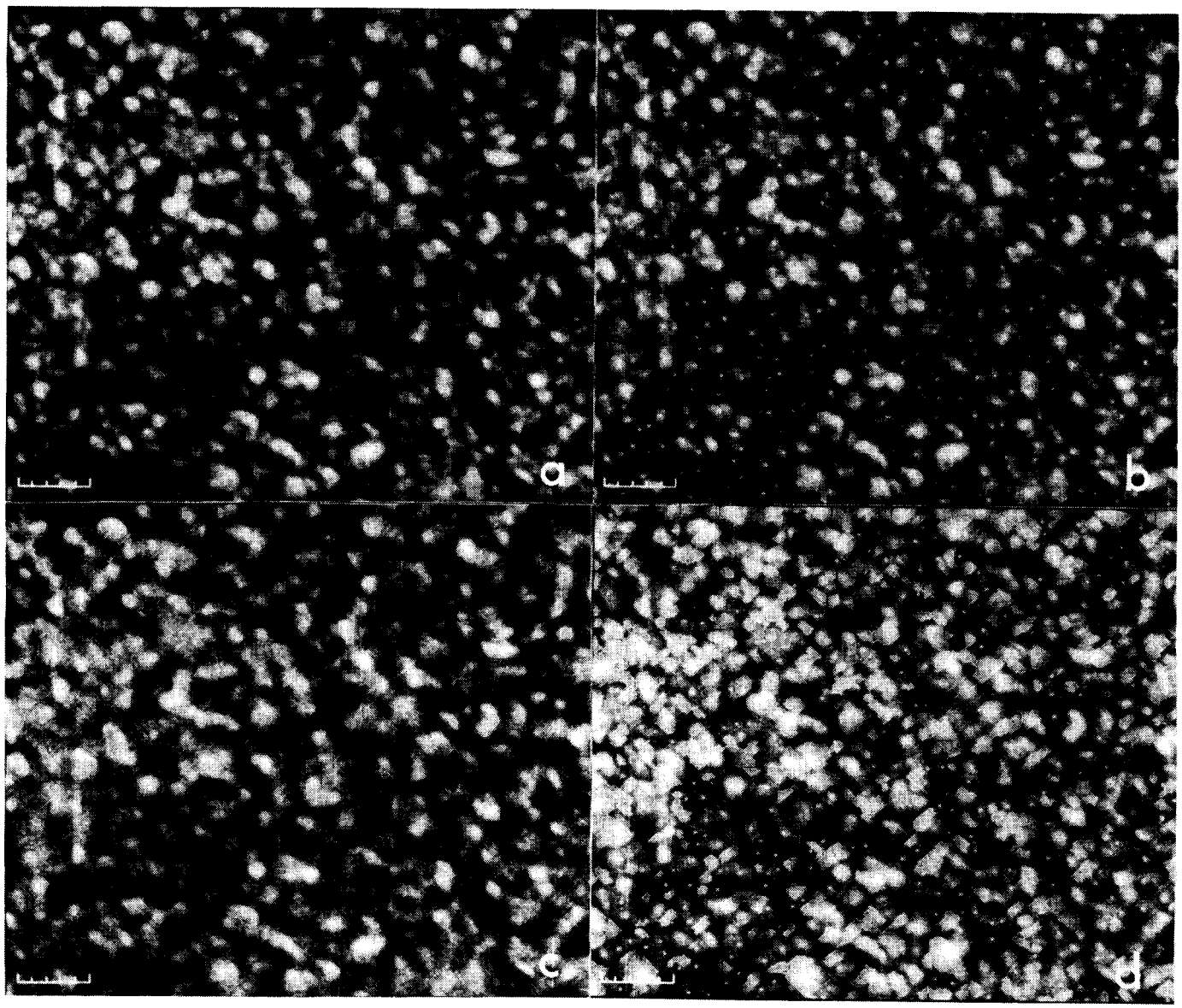

Fig. 11 Granule finding in quiet sun image (a), image with granule centers marked (b), image with lanes marked (c), and lane mesh shaded wherever a cell does not contain a center (d). The scale is marked in arc seconds.

ORIGINAL PAGE IS
OF POOR QUALITY

data. All of the plots are well fitted by an exponential decay,

$$N(t) = N_0 e^{-t/T},$$

where $N(t)$ is the number of granule strings of duration t, and T is the mean string lifetime. When $N(t) = 1/e,\ t = T$.

The center found granules yield a mean string lifetime of about five minutes, and the lane found granule strings have a somewhat shorter life. Increasing the value of M does not increase the apparent lifetime.

It was disapointing that the string finding procedures did not yield granule lifetimes longer that those measured by autocorrelation techniques; however, it was not suprising after viewing the movies which show many exploding granules and granules with apparent internal structure. The string lifetime result probably suggests that a significant fraction of granules fragment and then perhaps reform during a lifetime, and the simple procedure of following a center is not a sufficiently sophisticated algorthim for defining a granule history. It also suggests that granule evolution is not a simple central upwelling and boundary downflow. In the sections below we will discuss exploding granules and elongated granules which may offer some explanation of the lack of success of string finding, and give some insight into the evolutionary processes.

Although string finding has not been successful in finding a better measure of granule lifetimes, it has been very useful for measuring granule velocities. Each string connects the center of a granule or granule fragment as a function of time. We have fitted a straight line to the granule string paths and measured the slopes of these lines in space-time, and hence the velocity of the granule centers. Shown in figure 13 is the velocity, the $\pm 1\sigma$ velocity error, and the error of the mean as a function of string length-lifetime. There is some indication that short lived granules or granule fragments move faster than 1 km/s, but the error is rather large. However, it is hard to escape the fact that, on average, granules have a random velocity of 750 to 850 m/s.

The measurement of granulation size and evolution using tracking methods has not yet been done for magnetic sun. The original digitization operation in the pore region used 0.234 arc second pixels (quiet sun pixels are .161 arc seconds), which is not sufficent to reliably find granules using the techniques described here. We plan to redigitize the pore region data and carry out the analysis in the near future.

VI. Local Correlation Tracking

When unfiltered quiet sun movies are viewed, there are local centers that appear to be bubbling or upwelling. We took this appearance as visual evidence for the existence of local flows rather than some chance pattern in the p-mode oscillations. To study these flows we compared local regions in images separated in time by 60 seconds. A local region

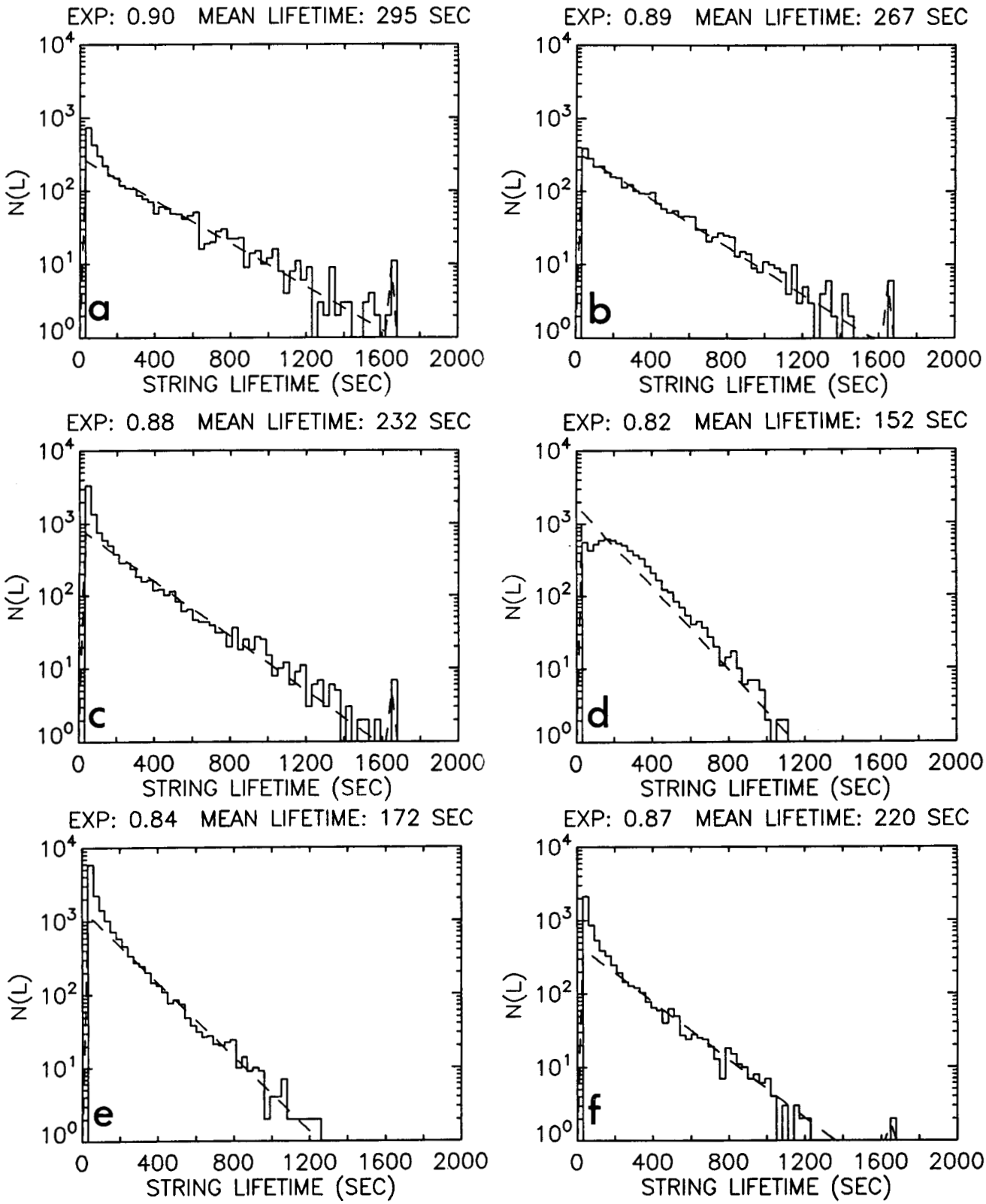

Fig. 12 Histograms of string lifetimes for subsonic data using center finding with M=0.5 arc second (a) and M=1 arc second (b); using lane finding (c) and (d); and for raw data using center finding (e) and string finding (f) with M=0.5 arc second.

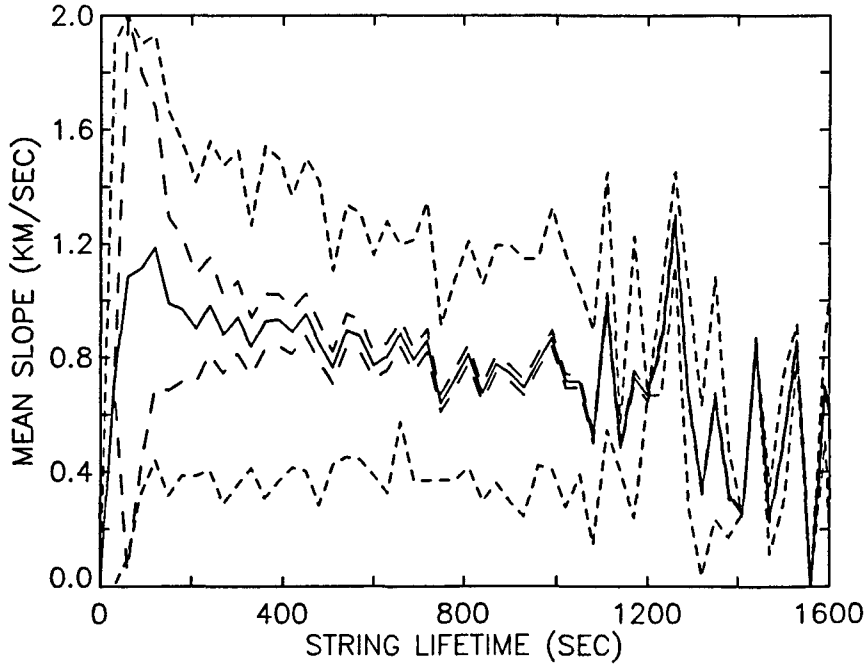

Fig. 13 Velocities from string slopes (solid), error of the mean (short dashes), and 1σ (long dashes).

was defined at a given image point by a mask centered at that point with a gaussian shape of 4 arc seconds diameter (FWHM). The mask function was set to zero outside an 8 arc second box. Before comparing locally, the full frames of each pair were aligned using a correlation algorithm. The mask was applied successively to a square grid with 2.5 arc second spacing (a 16×16 array) on the first image of a pair and then correlated with the second image to obtain the best fit. If the images had been identical a square grid of points with 2.5 arc second spacing on the second frame of the pair would have been found. Motions in the second image would cause the grid of best fit points to be distorted with respect to the first, and a displacement vector could be defined for each grid point.

The relative displacement field was obtained for 165 interleaved pairs of images each with 60 second spacing, and the average displacement field was computed. The largest displacements correspond to velocities of 1000 m/s and the average flow was 400 m/s. Figure 14a shows this displacement field overlayed on the average quiet sun image. The right hand side of the image appears to contain half of a supergranulation cell. In addition the image seems to be covered with smaller cells of size 10 to 15 arc seconds. The apparent cellular structure is accentuated when the mathematical divergence of the flow field is taken. (This is not the divergence of the solar flow because only the horizontal component is used.) Figure 14b shows the divergence field overlayed by the arrows.

We have used the flow maps to construct a synthetic time evolution of the surface flow. This was done by starting with a rectangular grid of tracers, "corks," at our grid intersections, and then subjecting the corks to the measured flow field. Initially the corks move in the direction of the arrows at their respective grid points, but as they displace they are moved by the flow field at their new positions. Cork frames at times of 0, 2.5, 5, and 7.5 hours

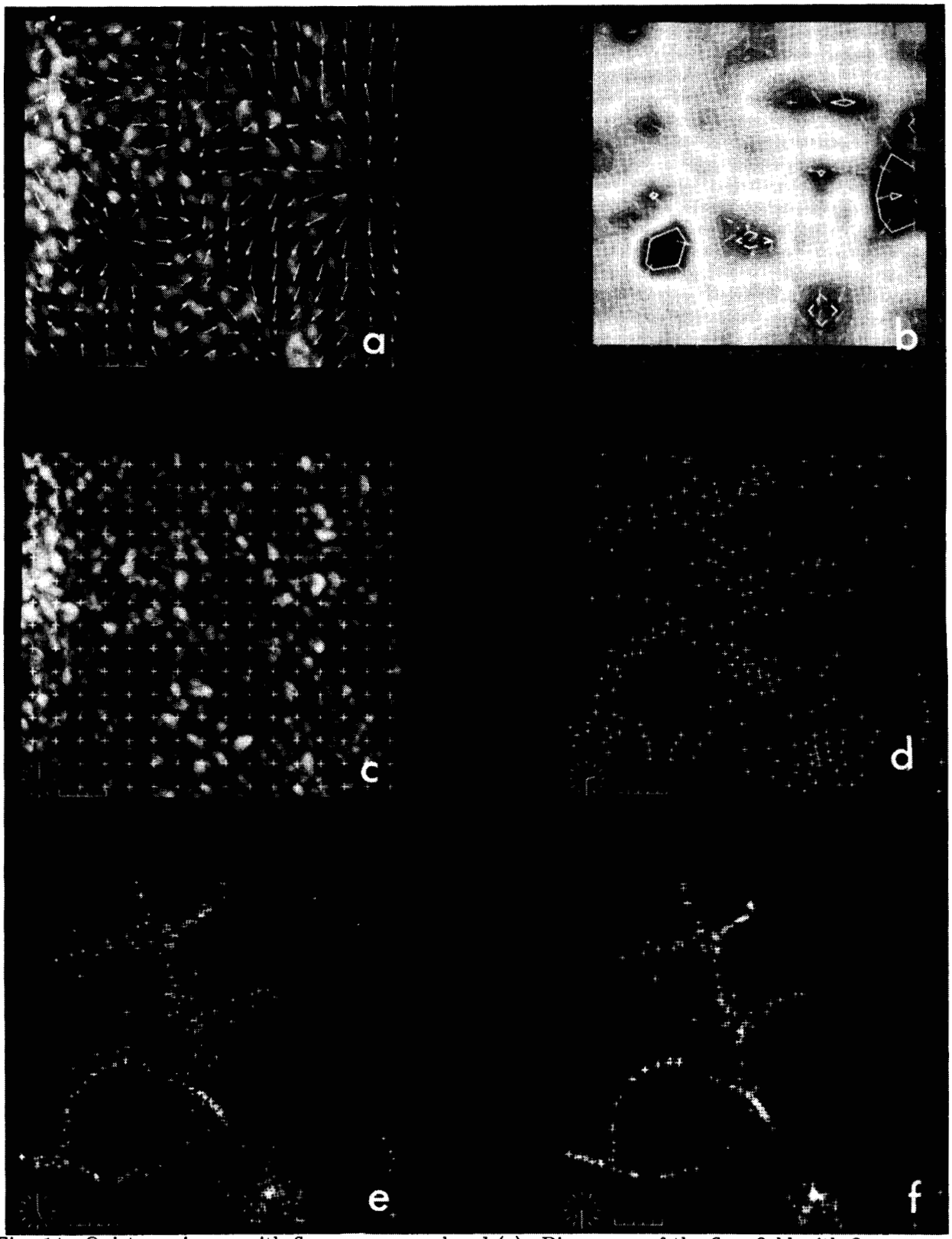

Fig. 14 Quiet sun image with flow arrows overlayed (a). Divergence of the flow field with flow arrows overlayed (b). Red areas are positive and blue areas are negative divergence. Quiet sun image overlayed by corks on a 2.5 arc second grid (c). Corks after 2.5 (d), 5 (e), and 7.5 (f) hours of being subject to the flow field.

ORIGINAL PAGE IS
OF POOR QUALITY

after release are shown in figures 14c, d, e, and f. The cork movie illustrates that the measured flows would create a "network" pattern, if they persisted for 6 to 10 hours. A current priority project is to measure how the actual flow pattern changes with time over the 16 hour interval for which we have SOUP data.

In the vicinity of the pores, the average flow field is significantly less than in the quiet sun. Figures 15a and b show the distribution of velocities for the quiet and pore regions. The area average velocity is 40 percent less in the pore region than quiet sun – 222 versus 368 m/s. Figure 16 shows a scatterplot of flow speed versus line of sight magnetic field. From the figure the flow averages about 100 m/s where the field is greater in magnitude than 100 gauss. Figures 17a and b show the velocity distribution functions in regions where the field is greater and less in magnitude than 100 gauss.

VII. Exploding Granules

Granules that appear to expand radially at the end of their lifetimes have been called exploding granules. A prototypical example is shown in figure 18. They are rather rare in groundbased granulation movies, but in SOUP data it is hard to find areas of quiet sun without them. Usually the ring is not a complete symmetrical structure, but rather an ensemble of local brightenings which are all traveling outward from a center. We have studied the 40×40 arc second quiet sun region intensively, and in it 44 (relatively isolated) examples of exploders can be recognized in the 1360 second movie.

Because the average diameter of the cells at maximum expansion is about 4 arc seconds, events which occur within 1.5 arc seconds of the edge of the frame are probably missed. In addition because it is hard to recognize an event unless the initial center or the final ring can be seen, a total of about 360 seconds at the beginning and end of the movie are lost for detection. Together these two effects amount to a correction factor of $(37/40)^2 \times (1000/1360) = .63$, which suggests that the movie most probably has about 70 exploders. Also, due to the relatively high density of exploders, some events will not be recognized because of overlap and interference. Using 70 events in 1360 seconds, at least one exploder is born in a 10×10 arc second area every 310 seconds.

The mean area of maximum expansion is 14.5 SAS, so that 1000 SAS, or 63 percent of the movie region are affected by exploders. When a granule explodes it "removes" $32 \times .145 = 4.7$ average granules. Thus, if the real granule lifetime is on the order of 10 minutes, about 1000 will have died in the duration of the movie, and 325, or 32 percent, may die because they were in the vicinity of "exploders." The exploding granule counts were based on a measurements of a movie smoothed by a 5 minute running average. When the subsonic filtered movie is observed, it is hard to find a granule that does not either explode or is not in the near vicinity of an exploder. In short, explosions are a major factor in determining the lifetime of granules in quiet sun.

We are using "time-slice" images to measure and quantify the behavior of individual granules. Imagine that all of the frames of the movie were glued together to make an (x, y, t) image cube. An individual granule in this cube would be a bright tube of some length and

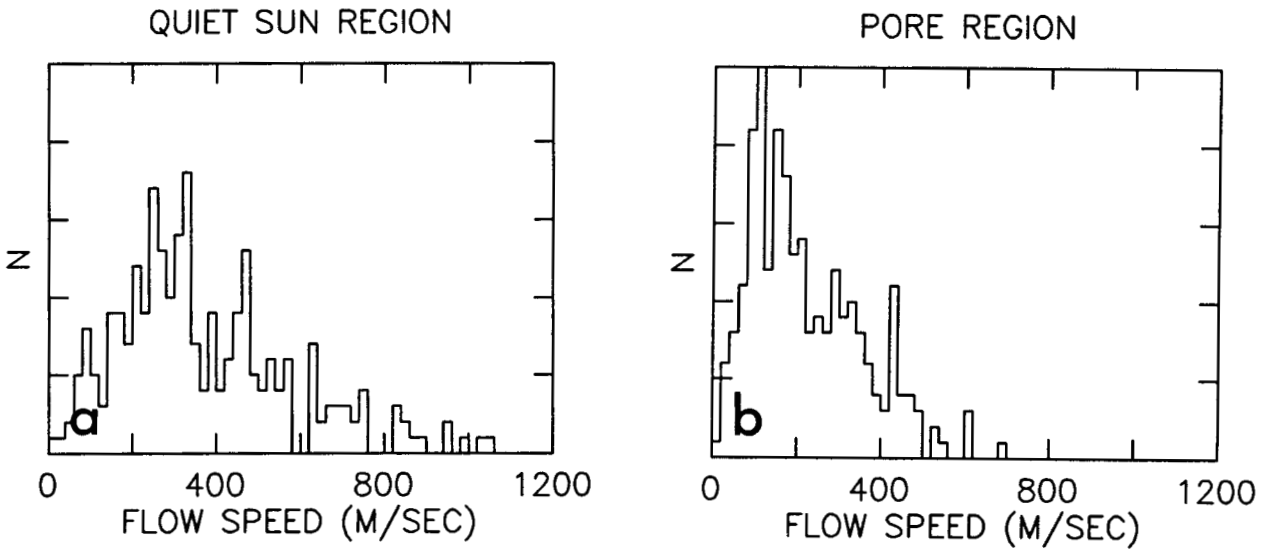

Fig. 15 Histogram of number (area) versus velocity in quiet (a) and pore (b) region.

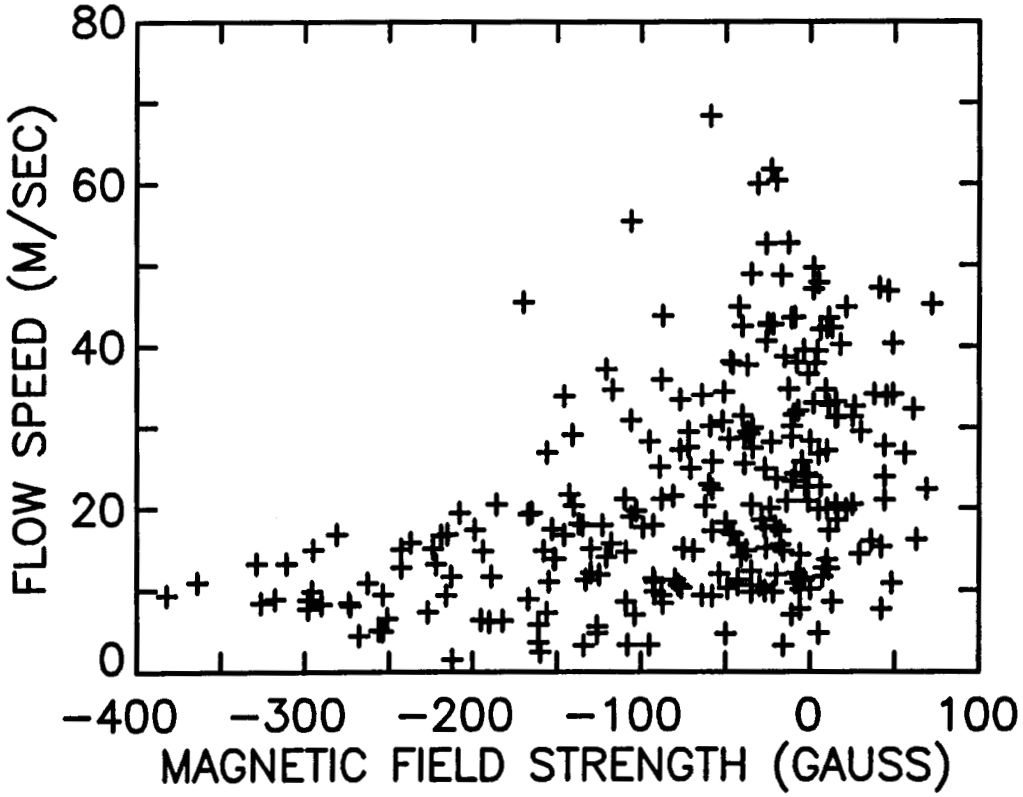

Fig. 16 Scatter plot of flow speed versus magnetic field strength.

ORIGINAL PAGE IS
OF POOR QUALITY

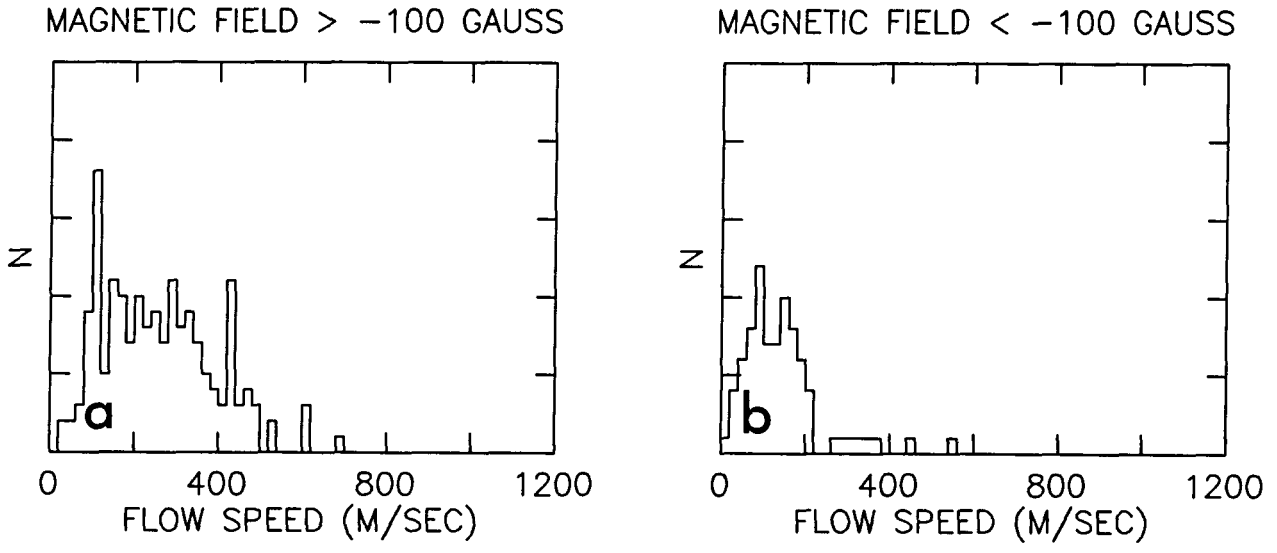

Fig. 17 Histograms of number (area) versus velocity in areas where the field strength is below (a) and above (b) |100| gauss.

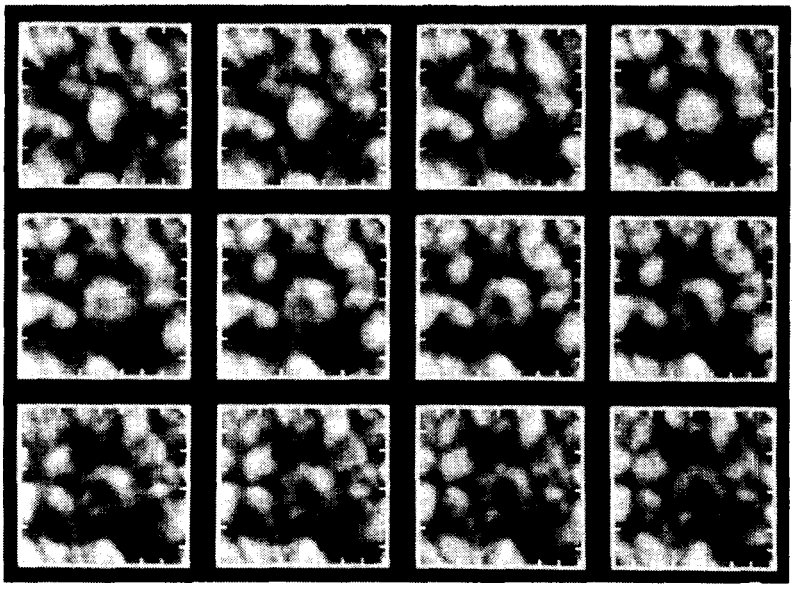

Fig. 18 Prototypical exploding granule time history. Tick marks are at arc second intervals and the time between frames is one minute.

inclination to the edges of the cube. An exploding granule would form a conical shell in the image cube. Imagine that the cube was placed on a slicing machine and was pushed into the slicer blade along the y spatial axis. As the slicer operated (x,t) slices at fresh values of y would be exposed. In the case of an exploding granule the slicer would expose a series of "V" shapes, and at the spatial center of the exploder the "V" would have its maximum opening angle. The tilt of the arms of the "V" is the radial expansion velocity of the exploder. Typical tilts correspond to velocities of about 1 km/s. Figure 19 shows slices through the center of five exploding granules.

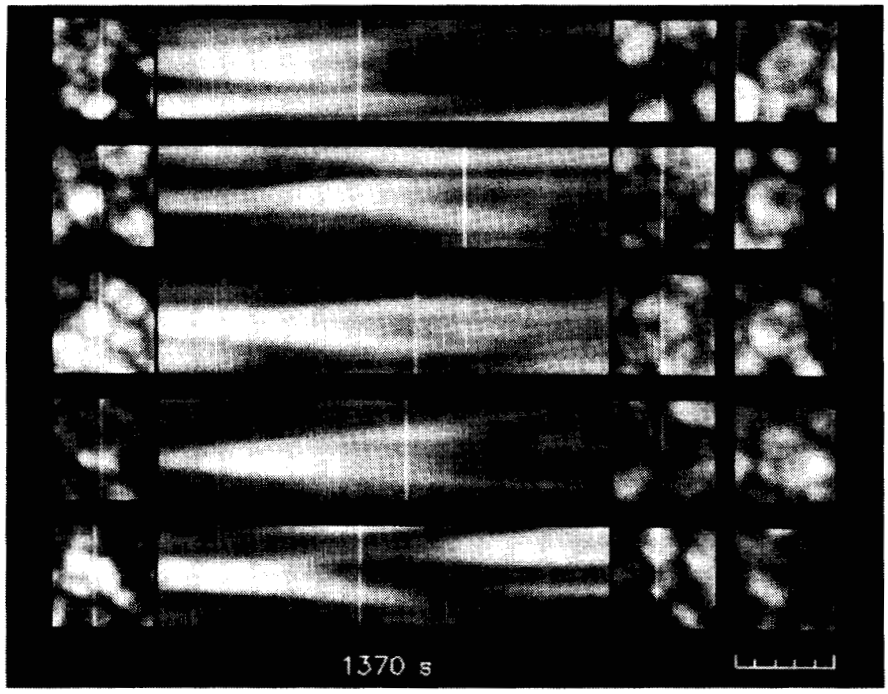

Fig. 19 Time slice images of five exploding granules.

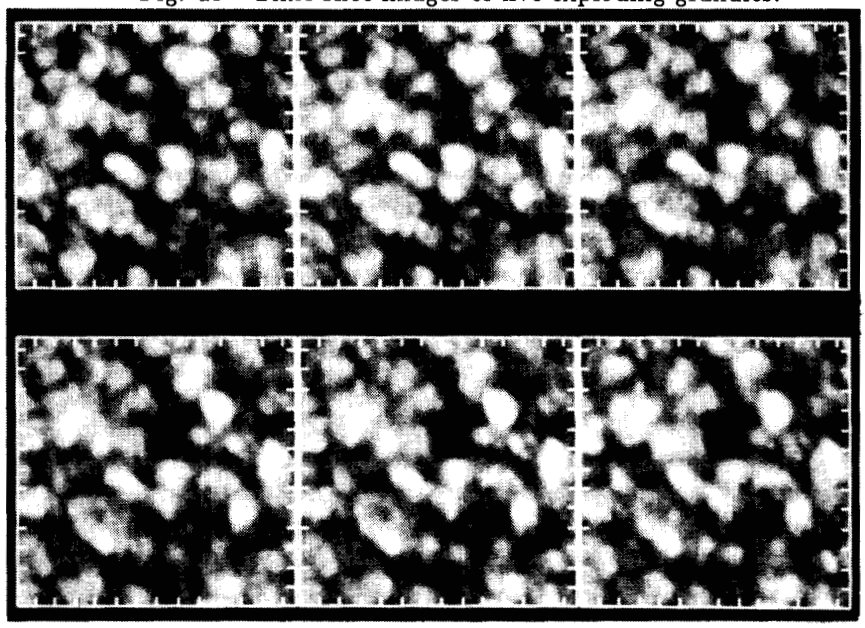

Fig. 20 Time sequence of images of region of elongated granules. Tick marks are at arc second intervals.

VIII. Elongated Granules

Figure 20 shows a sequence of frames with a number of granules that are elongated. Typical elongated granules are 0.5 × 1.5 arc seconds and appear in groups with their long axes parallel. From the illustration one gets the impression that the striations occur over an area much larger than a single granule. In at least one case we have observed a group of three elongated granules that turned into a single bright granule, and later dissolved back into a group of elongated granules. Our subjective impression is that the elongated

ORIGINAL PAGE IS
OF POOR QUALITY

granules are caused by a relatively stationary surface wave field in the photosphere. In rare cases striations appear to travel. These striations and their time evolution undoubtably play a significant role in complicating the definition of granules by an automated process.

Acknowledgements

Special thanks are extended to the crew of Spacelab 2 and the controllers and planners on the ground who worked so hard to get the observations . The SOUP experiment was supported by NASA under contract NAS8-23805. The image processing developments using laser optical disks has been supported by Lockheed Independent Research funds.

REFERENCES

Bray, R.J., Loughhead, R.E., and Durrant, C.J, 1984: *"The Solar Granulation,"* Cambridge University Press.

Mehltretter, J.P., 1978: *Astr. Astrophy.*, **62**, 311.

Mosher, J.M., 1977: PhD. Thesis, California Institute of Technology.

Namba, O., 1986: *Astr. Astrophy.*, **161**, 31.

Title, A.M., Tarbell, T.D., Simon, G.W., and the SOUP Team, 1986: *Advances in Space Res.*, in press.

Wittmann, A., 1979: *"Small Scale Motions on the Sun,"* Kiepenheuer-Institut für Sonnenphysik.